frontiers | Frontiers in Energy Research

TYPE Original Research
PUBLISHED 30 October 2024
DOI 10.3389/fenrg.2024.1481205

OPEN ACCESS

EDITED BY
Howard Qingsong Tu,
Rochester Institute of Technology (RIT),
United States

REVIEWED BY
Fengyu Shen,
Berkeley Lab (DOE), United States
Jie Zheng,
University of Houston, United States

*CORRESPONDENCE
Nguyen Huu Huy Phuc,
nhhphuc@hcmut.edu.vn

RECEIVED 15 August 2024
ACCEPTED 24 October 2024
PUBLISHED 30 October 2024

CITATION
Minh Nguyet NT, Anh LT, Toan TV, Tu TA, Quynh Anh LT and Huy Phuc NH (2024) Liquid-phase synthesis of a Li_3PS_4 solid electrolyte using ethyl isobutyrate as a synthetic medium.
Front. Energy Res. 12:1481205.
doi: 10.3389/fenrg.2024.1481205

Liquid-phase synthesis of a Li_3PS_4 solid electrolyte using ethyl isobutyrate as a synthetic medium

Nguyen Thi Minh Nguyet[1,2], Luu Tuan Anh[2,3], Tran Viet Toan[2,3], Tran Anh Tu[2,3,4], Luong Thi Quynh Anh[2,3] and Nguyen Huu Huy Phuc[2,3,4]*

[1]VNU-HCM Key Laboratory for Material Technologies, Ho Chi Minh City University of Technology (HCMUT), Ho Chi Minh City, Vietnam, [2]Vietnam National University Ho Chi Minh City, Ho Chi Minh City, Vietnam, [3]Faculty of Materials Technology, Ho Chi Minh City University of Technology (HCMUT), Ho Chi Minh City, Vietnam, [4]National Key Laboratory of Polymer and Composite Materials – Ho Chi Minh City, Ho Chi Minh City, Vietnam

A β-Li_3PS_4 solid electrolyte was prepared via liquid-phase synthesis using ethyl isobutyrate as a synthetic medium. The precursor and solid electrolyte structures were characterized using thermogravimetry–differential thermal analysis and X-ray diffraction techniques. The dielectric relaxation analysis showed two relaxation regions, which revealed a bulk and grain boundary ionic migration process. At a temperature lower than 90°C, the frequency dependence of the dielectric constant of the prepared sample was different from that of glassy Li_3PS_4, indicating that the motion of the PS_4 unit enhances the ionic conductivity of the Li_3PS_4 solid electrolyte. The ionic conductivities of the cold-pressed and warm-pressed pellets at 25°C were 6.8×10^{-5} Scm^{-1} and 3.6×10^{-4} Scm^{-1}, respectively.

KEYWORDS

Li_3PS_4 solid electrolyte, liquid-phase synthesis, complex impedance spectroscopy, grain-boundary, ionic conductivity

1 Introduction

All-solid-state batteries are promising candidates for use in electric vehicles, aiming to contribute to a sustainable society (Bates et al., 2022; Lu et al., 2022; Schmaltz et al., 2023). Solid electrolytes are key components in all-solid-state batteries. Intensive research efforts have been conducted on oxides, sulfides, and polymer-based electrolytes to find the most suitable for solid-state batteries. Li_3PS_4 is the most common electrolyte among sulfur-based solid electrolytes. Li_3PS_4 exhibits three temperature-dependent polymorphic forms: α-Li_3PS_4 at high temperatures, β-Li_3PS_4 at medium temperatures, and γ-Li_3PS_4 at low temperatures. The β-Li_3PS_4 phase crystallized from heat-treated Li_3PS_4 glass becomes stable at room temperature (Ohtomo et al., 2013). Glassy Li_3PS_4 and β-Li_3PS_4 stabilized in glass matrix are well-known model materials that have been employed to investigate the relationship between structure and ionic conductivity. Recently, α-Li_3PS_4

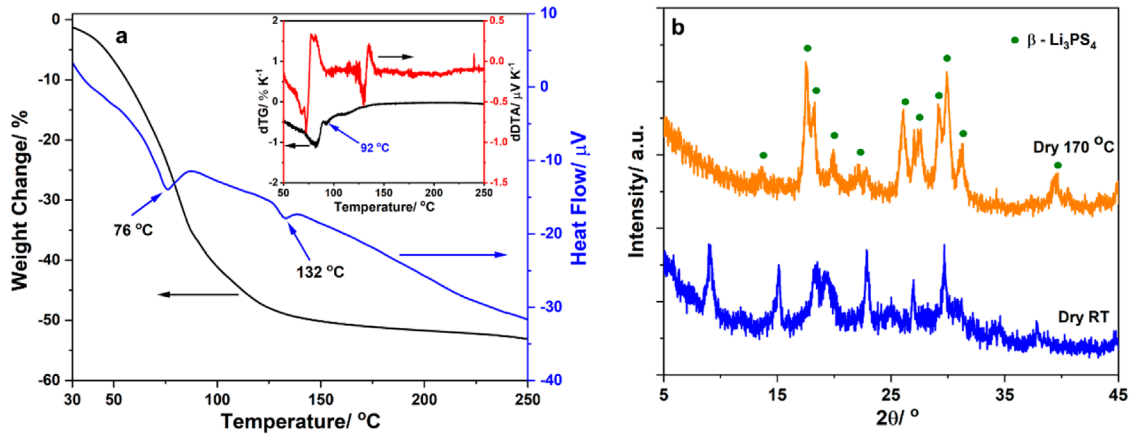

FIGURE 1
(A) Thermogravimetry–differential thermal analysis (TG–DTA) curves of the Li_3PS_4 precursor obtained after ethyl isobutyrate (EiB) removal at room temperature and their derivatives (inset); **(B)** X-ray diffraction (XRD) patterns of the Li_3PS_4 precursor obtained after EiB removal at room temperature and β-Li_3PS_4 obtained after precursor heat treatment at 170°C.

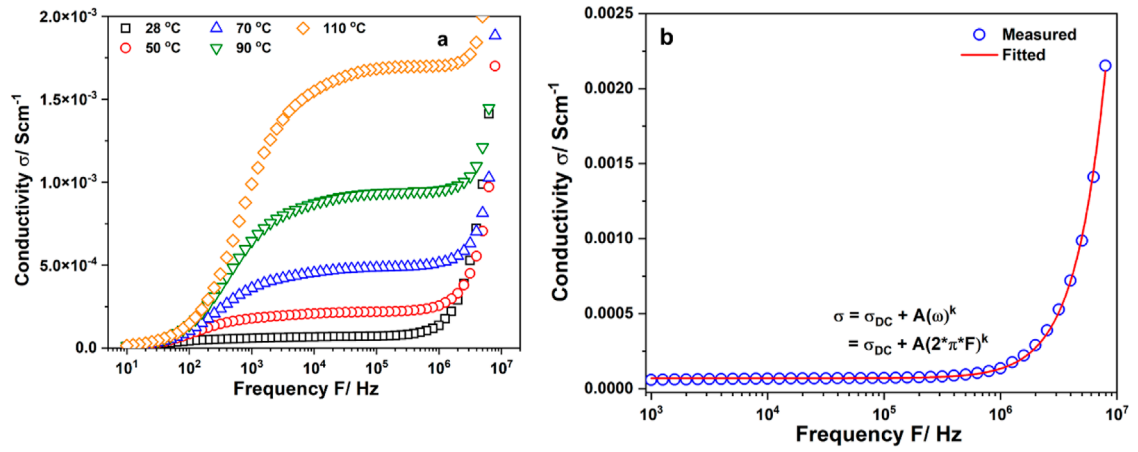

FIGURE 2
(A) Conductivity isotherms of EiB Li_3PS_4; **(B)** Fitting of conductivity isotherm at 28°C using Jonscher's power law.

was stabilized in a glass–ceramic structure and exhibited an ionic conductivity higher than 10^{-3} Scm^{-1} at room temperature (Kimura et al., 2023).

The ionic conductivity of glassy Li_3PS_4, which is often prepared using the planetary ball milling method, is ~3.0×10^{-4} Scm^{-1} at room temperature (Phuc et al., 2022), and that of the well-crystalline β-Li_3PS_4 is ~1.6×10^{-4} Scm^{-1} (Stöffler et al., 2019). The liquid-phase synthesis of Li_3PS_4 has attracted significant attention because the formed solid electrolyte suspension or solution can be directly applied to the battery preparation process (Gamo et al., 2022; Gamo et al., 2023). Tetrahydrofuran, ethyl acetate, acetonitrile, and pyridine have been employed as synthetic media to prepare the β-Li_3PS_4 solid electrolyte (Liu et al., 2013; Phuc et al., 2016; Calpa et al., 2021; Ghidiu et al., 2021). In addition, several studies showed that Li_2S reacts with P_2S_5 in organic solvents via a multistep reaction to form a Li_3PS_4 precursor and is transformed into a Li_3PS_4 solid electrolyte after solvent elimination (Phuc et al., 2017a; Calpa et al., 2020). The ionic conductivity of the Li_3PS_4 solid electrolyte, which is prepared via a liquid-phase synthesis, is lower than that of the amorphous Li_3PS_4 obtained using planetary ball milling. This is attributed to the formation of crystalline Li_3PS_4 during solvent elimination (Takahashi et al., 2021); another reason, is solvent residue (Yamamoto et al., 2020). The ionic conductivity of a low-crystalline Li_3PS_4 solid electrolyte produced from butyl acetate is ~5.09×10^{-4} Scm^{-1} at 25°C, which was comparable to that of glassy Li_3PS_4 (Yamamoto et al., 2021).

Broadband dielectric spectroscopy is used to describe the dielectric dispersion and absorption phenomena due to dipole relaxation and electrical conduction over a wide frequency range (10^{-6}–10^{12} Hz), which corresponds to a timescale from a few picoseconds to hours. AC EIS is typically used for frequencies in the 10 Hz–10 MHz range. EIS is a suitable and inexpensive measurement method, which is used in low-frequency and low-impedance ranges. Therefore, it is suitable for the characterization of materials with time-dependent dielectric properties. The complex

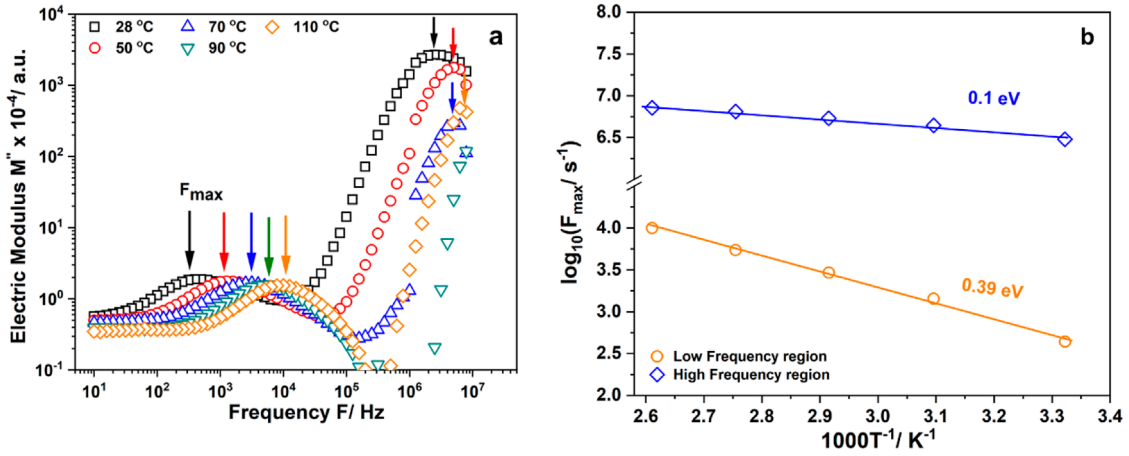

FIGURE 3
(A) Variation of imaginary part of the electric modulus (M″) with frequency of EiB Li_3PS_4; **(B)** Temperature dependence of inversed relaxation time.

dielectric constant ε*, complex impedance Z*, complex electric modulus M*, and tangent loss (tanδ) are the frequency-dependent electrical properties of materials; these parameters can be extracted from EIS measurements and provide important knowledge about the performance of localized charge carriers in the sample. The complex conductivity, σ*, of samples was determined from the complex impedance, Z*:

$$\sigma^* = \sigma' + j\sigma'' = \frac{l}{AZ^*} = \frac{l}{AZ'} + j\frac{l}{AZ''}$$

where A (cm^2) and l (cm) are the contact area and the thickness of the pellets, respectively.

In the electric modulus formalism, the complex electric modulus $M^*(\omega)$ is defined by:

$$M^* = \frac{1}{\varepsilon^*} = \frac{\varepsilon' - j\varepsilon''}{|\varepsilon^*|^2} = M' + jM'' = \frac{\varepsilon'}{\varepsilon'^2 + \varepsilon''^2} - j\frac{\varepsilon''}{\varepsilon'^2 + \varepsilon''^2}$$

$$\varepsilon^* = \varepsilon' - j\varepsilon'' = \frac{\sigma'}{\omega\varepsilon_0} - j\frac{\sigma''}{\omega\varepsilon_0}$$

where ω (= 2πf, radians/second) is a radial frequency and ε_0 is the permittivity of free space.

Although several studies on the liquid-phase synthesis of the Li_3PS_4 solid electrolyte have been reported in the literature, there is still a lack of knowledge on the Li ion movement in a Li_3PS_4 solid electrolyte prepared via liquid-phase synthesis. Solvents containing ester functional groups, such as ethyl acetate, ethyl propionate, methyl propionate, and butyl acetate, have been used to synthesize Li_3PS_4 (Phuc et al., 2016; Yamamoto et al., 2021; Phuc et al., 2017b; Phuc et al., 2019). To the best of our knowledge, the synthesis of Li_3PS_4 using ethyl isobutyrate, which features the ester functional group, has not been reported in the literature. In this work, a Li_3PS_4 solid electrolyte was prepared via liquid-phase synthesis using ethyl isobutyrate (EiB) as a reaction medium, and the electrical properties of the electrolyte were investigated to understand the ionic transport mechanism in the temperature range from room temperature to 110°C.

2 Experimental

2.1 Chemicals

Li_2S (99.9%, Aldrich), P_2S_5 (99%, Merck), and super dehydrated EiB (Aldrich) were used as received without further treatment.

2.2 Liquid-phase synthesis of Li_3PS_4

Initially, 1.5 g of Li_2S and P_2S_5 (a 75:25 M ratio) was weighed and put into a screw vial together with 40 mL of EiB. The mixture was stirred at 400 rpm and heated at 50°C for 24 h. Then, the solvent was evaporated at room temperature. The residue was carefully grounded using an agate mortar before heat treatment to obtain the Li_3PS_4 solid electrolyte. The sample is denoted as EiB Li_3PS_4.

2.3 Structural characterization

The structures of the prepared samples were characterized using thermogravimetry–differential thermal analysis (TG–DTA; EVO II, Rigaku), and X-ray diffraction (XRD; X8, Bruker).

2.4 AC electrochemical impedance spectroscopy

Electrical conductivity measurements were performed on a pellet (~10.0 mm in diameter) prepared via uniaxially cold pressing; ~100 mg of powder was subjected to 510 MPa pressure. The pellet was placed in a holder made of polycarbonate with two stainless steel rods as blocking electrodes. The stack pressure was about 110 MPa. Alternating current (AC) electrochemical

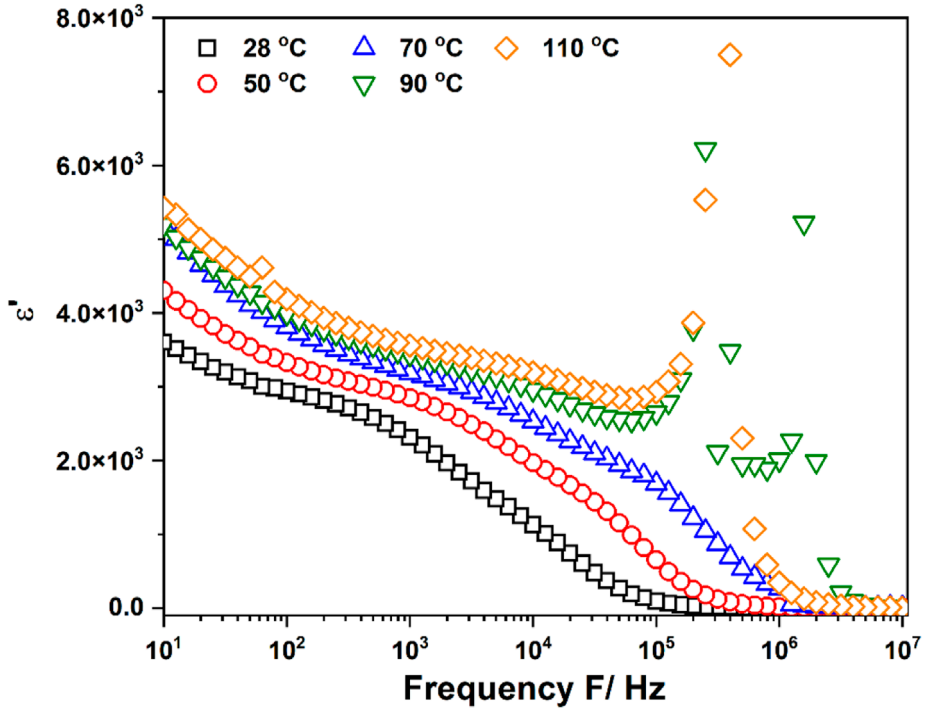

FIGURE 4
Frequency dependence of the real part of the dielectric constant (ε′) with frequency for EiB Li_3PS_4.

impedance spectroscopy (EIS) measurements were performed using a potentiostat (PGSTAT302N, Autolab, Herisau, Switzerland) in the 9 MHz–10 Hz range.

All the experiments were carried out in a glove box (Ar-filled [H_2O] < 0.1 ppm) or an airtight sample holder.

3 Results and discussion

Figure 1A shows the TG–DTA curve of the powder obtained from the reaction mixture at room temperature after solvent elimination. The DTA curve exhibits two intense endothermic peaks centered at 76°C and 132°C, respectively. Since the boiling point of EiB is ~110°C, the DTA results indicate that EiB was chemically bonded in the sample. The TG curve exhibits a plateau starting at ~150°C after the sample has lost ~50% of its initial mass due to EiB evaporation. We calculated the first-order derivatives of the TG–DTA curves (inset of Figure 1A) to further analyze the TG–DTA results. The derivative of the TG curve shows that the mass loss occurs in two simultaneous steps with two endothermic troughs shown in the derivative of the DTA curve. The first step ends at ~92°C and corresponds to ~33% mass loss. The second occurs after that and ends at ~150°C and corresponds to ~17% mass loss. The estimated formulas of the sample in the first and second trough are Li_3PS_4·1EiB and 2Li_3PS_4·1EiB, respectively. Overall, the formula of the sample obtained after EiB removal at room temperature is 3Li_3PS_4·2EiB. This ratio is different from that of the powder prepared using ethyl acetate (Li_3PS_4·2 EA) and shows the effect of the organic solvent structure on the synthesis of Li_3PS_4 (Phuc et al., 2016). The TG–DTA results show that the appropriate temperature for removing EiB from the precursor to obtain the Li_3PS_4 solid electrolyte is 170°C. Thus, the samples were heat treated at 170°C for 1 h and cooled down naturally at room temperature to obtain EiB Li_3PS_4.

Figure 1B shows the XRD patterns of the precursor and EiB Li_3PS_4. The 3Li_3PS_4·2EiB pattern exhibits many peaks; thus, it cannot be assigned to any known phases. In addition, this pattern resembles that of the Li_3PS_4 precursor, which was prepared using ethyl propionate (Phuc et al., 2017b). The EiB Li_3PS_4 pattern can be matched with that of β-Li_3PS_4. This is consistent with the structure of the liquid-phase synthesized Li_3PS_4 solid electrolyte (Calpa et al., 2021; Takahashi et al., 2021). Therefore, we conclude that EiB was effectively removed after heat treatment at 170°C for 1 h.

Figure 2A shows the frequency dependence of the real part σ′ of the complex conductivity of EiB Li_3PS_4. The conductivity isotherms of the sample exhibits temperature dependence. The conductivity isotherms had electrode polarization at low frequencies, polarization conductivity at high frequencies, and a plateau in the intermediate frequency region. Electrode polarization is caused by the accumulation of ions at the blocking electrodes (Preishuber-Pflugl and Wilkening, 2016). The conductivity in the intermediate frequency region can be expressed as $\sigma = \sigma_{DC} + A\,\omega^k$ (Jonscher power law), where σ_{DC} is the direct current (DC) conductivity, A is a pre-factor, and k is the frequency exponent in the $0 < k < 1$ range (Jonscher and White, 1979; Funke, 1997). The DC conductivity

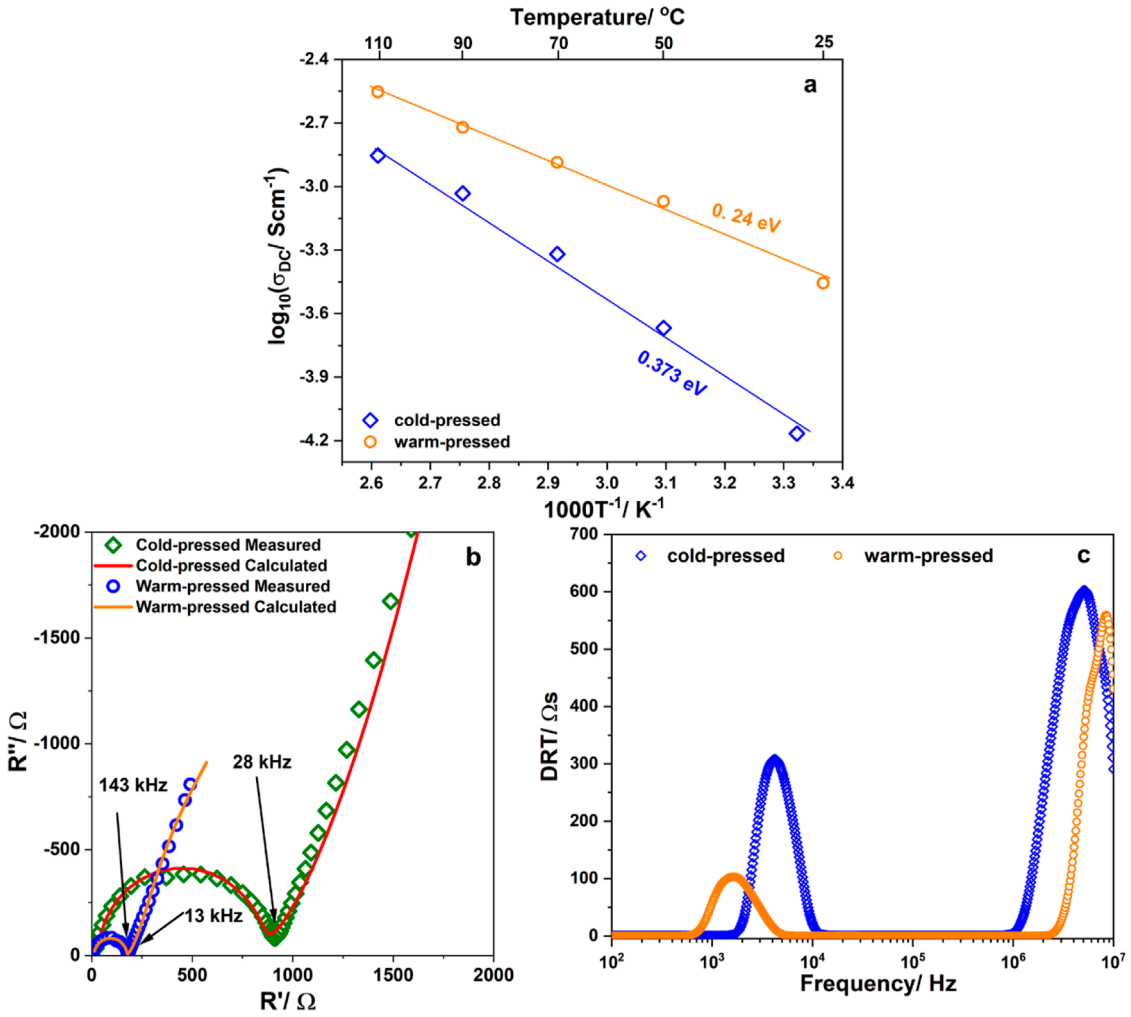

FIGURE 5
(A) Temperature dependence of the ionic conductivity of the cold- and warm-pressed EiB Li_3PS_4 pellets at room temperature and at 170°C, respectively; **(B)** corresponding Nyquist plots with small inset showing equivalent circuit model; **(C)** corresponding distribution of relaxation time (DRT) (the insets illustrate the resistance contribution of the grain boundary (GB) and bulk regions to the total resistance.

exhibits long-range ion transport and temperature dependence of σ_{DC}, indicating that the charge carrier concentration increases with temperature. σ_{DC} was obtained for each temperature by fitting the conductivity curves using the above equation. Figure 2B shows the fitting result of conductivity measured at room temperature. It could be seen that the conductivity of the sample followed Jonscher power law.

The relaxation process is the result of the transition from correlated to uncorrelated ion hopping. The electric modulus represents the relaxation of the electric field in a material with a constant electric displacement. The variation of the imaginary part M'' of the complex modulus of EiB Li_3PS_4 against frequency is shown in Figure 3A. The conductivity becomes very high at high temperatures (above 90°C), and the peaks are not fully visible. The region on the left of F_{max} (which is equal to the inverse relaxation time) shows the movement of charge carriers, and the region on the right is the region where ions are spatially confined within their potential wells. The Li ion movement in EiB Li_3PS_4 is observed in the 10^5–10^7 Hz and 10^2–10^5 Hz frequency regions. The relaxation time $t_{M''}$ is defined as the most probable conductivity relaxation time of the ions. The dependence of inverse relaxation time ($t_{M''}^{-1} = F_{max}$) on the inverse temperature is shown in Figure 3B. The activation energy for relaxation at low- and high-frequency regions are 0.39 and 0.10 eV, respectively.

Figure 4 shows the dependence of the real part of the dielectric constant ε' of EiB Li_3PS_4 on frequency for different temperatures. In all plots, the increase in the low-frequency region can be attributed to the electrode–electrolyte interface polarization due to the accumulation of ions near the electrode; this leads to the formation of the space charge layer, which, in turn, blocks the electric field and enhances the electrical polarization. The dielectric constant decreases with frequency. In all samples, ε' increases with temperature, indicating that the charge carrier movement is thermally activated. The EiB Li_3PS_4 plots at room temperature, 50°C, and 70°C exhibit a continuously decreasing trend in the intermediate and high-frequency regions. The maxima are observed at 90°C and

110. The change in the shape of the ε' plots indicates a change in the EiB Li_3PS_4 microstructure and this process was temperature dependence.

Figure 5A shows the dependence of the DC conductivities of EiB Li_3PS_4 on the inverse temperature. Both the bulk and grain boundary (denoted as GB) resistances contribute to the σ_{DC} value. It was observed that $\log_{10}(\sigma_{DC})$ follows the Arrhenius equation $\sigma_{DC} = \sigma_0 \exp(-E_{a,DC}/[k_B T])$. The ionic conductivities of EiB Li_3PS_4 at 25°C was about 6.8×10^{-5} Scm^{-1} and the activation energy was about 36 kJ mol^{-1}. The ionic conductivity of EiB Li_3PS_4 obtained in this study is of the same order as that of β-Li_3PS_4 prepared using pyridine (Ghidiu et al., 2021). The activation energy value obtained from the dependence of the relaxation time on temperature in the low-frequency region (Figure 3B) was close to the conduction value, indicating that the activation energy for the Li ion movement in the GB is the main component of the DC activation energy. Those results indicated that the GB resistance was the main issue in the EiB Li_3PS_4 ionic conductivity at room temperature; thus, the pellet of this sample was warm-pressed at 170°C and 60 MPa for 1 h to reduce the GB resistance. The temperature dependence of the ionic conductivity of the cold-pressed and warm-pressed pellets is shown in Figure 5B and denoted as "cold-pressed" and "warm-pressed," respectively. We observed that the ionic conductivity at 25°C had been significantly improved from 6.8×10^{-5} to 3.6×10^{-4} Scm^{-1}. The activation energies for the Li ion movement in the cold-pressed and warm-pressed pellets are 0.373 eV and 0.24 eV, respectively. The resistance components of the cold-pressed and warm-pressed pellets were double checked using the distribution relaxation time (DRT) (Wan et al., 2015). The Nyquist plots with small inset showing equivalent circuit model and DRT spectra of the cold-pressed and warm-pressed EiB Li_3PS_4 pellets measured at room temperature are shown in Figures 5B, C, respectively. Each of the DRT spectra of the cold-pressed and warm-pressed pellets exhibit two peaks located in the low- and high-frequency regions, indicating the contribution of GB and bulk resistances to the ionic conductivity of the samples. The insets in Figure 5C show the contributions of GB and bulk resistances to the total resistance of each sample. The GB resistance contribution to the total resistance of the cold-pressed pellet is ~27%; however, that of the warm-pressed pellet is ~15%. The ratio between GB resistances in warm-pressed and cold-pressed pellets was about 15%. The ratio between bulk resistances in warm-pressed and cold-pressed pellets was about 79%. Thus, the warm pressing process reduced most of the resistance at the grain boundary.

4 Conclusion

A Li_3PS_4 solid electrolyte was successfully prepared using EiB as a synthetic medium. The TG results showed that the formula of the solid electrolyte precursor was $3Li_3PS_4 \cdot 2EiB$. β-Li_3PS_4 was obtained after solvent elimination from the precursor at 170°C. The ionic conductivity of the cold-pressed pellet at 28°C was ~6.8×10^{-5} Scm^{-1}. The conductivity of the warm-pressed pellet at 25°C was ~3.6×10^{-4} Scm^{-1}, which was close to that of glassy Li_3PS_4. Two relaxation peaks at low and high frequencies indicated the concept of GB and bulk conduction. The relaxation activation energy was close to the activation energy obtained from the DC conductivity, indicating that the lithium-ion movement was responsible for both the ionic conduction and the relaxation process.

Data availability statement

The original contributions presented in the study are included in the article/supplementary material, further inquiries can be directed to the corresponding author.

Author contributions

NM: Data curation, Formal Analysis, Investigation, Writing–review and editing. LA: Data curation, Investigation, Writing–review and editing. TTo: Formal Analysis, Investigation, Methodology, Validation, Writing–review and editing. TTu: Data curation, Investigation, Methodology, Resources, Software, Validation, Writing–original draft. LQ: Formal Analysis, Investigation, Methodology, Supervision, Validation, Writing–review and editing. NH: Conceptualization, Investigation, Supervision, Validation, Visualization, Writing–original draft, Writing–review and editing.

Funding

The author(s) declare that no financial support was received for the research, authorship, and/or publication of this article.

Acknowledgments

We acknowledge Ho Chi Minh City University of Technology (HCMUT), VNU-HCM for supporting this study. We thank Ruediger (Enago; https://www.enago.com/vnuhcm/) for the English language review.

Conflict of interest

The authors declare that the research was conducted in the absence of any commercial or financial relationships that could be construed as a potential conflict of interest.

Publisher's note

References

Bates, A. M., Preger, Y., Torres-Castro, L., Harrison, K. L., Harris, S. J., and Hewson, J. (2022). Are solid-state batteries safer than lithium-ion batteries? *Joule* 6, 742–755. doi:10.1016/j.joule.2022.02.007

Calpa, M., Nakajima, H., Mori, S., Goto, Y., Mizuguchi, Y., Moriyoshi, C., et al. (2021). Formation mechanism of β-Li_3PS_4 through decomposition of complexes. *Inorg. Chem.* 60, 6964–6970. doi:10.1021/acs.inorgchem.1c00294

Calpa, M., Rosero-Navarro, N. C., Miura, A., Terai, K., Utsuno, F., and Tadanaga, K. (2020). Formation mechanism of thiophosphate anions in the liquid-phase synthesis of sulfide solid electrolytes using polar aprotic solvents. *Chem. Mater.* 32, 9627–9632. doi:10.1021/acs.chemmater.0c03198

Funke, K. (1997). Ion transport in fast ion conductors - spectra and models. *Solid State Ionics* 94, 27–33. doi:10.1016/s0167-2738(96)00500-0

Gamo, H., Nagai, A., and Matsuda, A. (2023). Toward scalable liquid-phase synthesis of sulfide solid electrolytes for all-solid-state batteries. *Batteries* 9, 355. doi:10.3390/batteries9070355

Gamo, H., Nishida, J., Nagai, A., Hikima, K., and Matsuda, A. (2022). Solution processing via dynamic sulfide radical anions for sulfide solid electrolytes. *Adv. Energy Sustain. Res.* 3, 2200019. doi:10.1002/aesr.202200019

Ghidiu, M., Schlem, R., and Zeier, W. G. (2021). Pyridine complexes as tailored precursors for rapid synthesis of thiophosphate superionic conductors. *Batter. and Supercaps* 4, 607–611. doi:10.1002/batt.202000317

Jonscher, K. L. N. A. K., and White, C. T. (1979). On the origin of the universal dielectric response in condensed matter. *Nature* 277, 185–189. doi:10.1038/277185a0

Kimura, T., Inaoka, T., Izawa, R., Nakano, T., Hotehama, C., Sakuda, A., et al. (2023). Stabilizing high-temperature α-Li_3PS_4 by rapidly heating the glass. *J. Am. Chem. Soc.* 145, 14466–14474. doi:10.1021/jacs.3c03827

Liu, Z., Fu, W., Payzant, E. A., Yu, X., Wu, Z., Dudney, N. J., et al. (2013). Anomalous high ionic conductivity of nanoporous β-Li_3PS_4. *J. Am. Chem. Soc.* 135, 975–978. doi:10.1021/ja3110895

Lu, Y., Zhao, C.-Z., Yuan, H., Hu, J.-K., Huang, J.-Q., and Zhang, Q. (2022). Dry electrode technology, the rising star in solid-state battery industrialization. *Matter* 5, 876–898. doi:10.1016/j.matt.2022.01.011

Ohtomo, T., Hayashi, A., Tatsumisago, M., Tsuchida, Y., Hama, S., and Kawamoto, K. (2013). All-solid-state lithium secondary batteries using the 75Li2S·25P2S5 glass and the 70Li2S·30P2S5 glass–ceramic as solid electrolytes. *J. Power Sources* 233, 231–235. doi:10.1016/j.jpowsour.2013.01.090

Phuc, N. H. H., Gamo, H., Hikima, K., Muto, H., and Matsuda, A. (2022). Novel (100-x-y)Li3PS4-xLiBF4-yLiCl amorphous solid electrolytes for all-solid-state Li ion battery. *J. Non-Crystalline Solids* 593, 121768. doi:10.1016/j.jnoncrysol.2022.121768

Phuc, N. H. H., Morikawa, K., Mitsuhiro, T., Muto, H., and Matsuda, A. (2017b). Synthesis of plate-like Li3PS4 solid electrolyte via liquid-phase shaking for all-solid-state lithium batteries. *Ionics* 23, 2061–2067. doi:10.1007/s11581-017-2035-8

Phuc, N. H. H., Muto, H., and Matsuda, A. (2019). Fast preparation of Li3PS4 solid electrolyte using methyl propionate as synthesis medium. *Mater. Today Proc.* 16, 216–219. doi:10.1016/j.matpr.2019.05.286

Phuc, N. H. H., Totani, M., Morikawa, K., Muto, H., and Matsuda, A. (2016). Preparation of Li3PS4 solid electrolyte using ethyl acetate as synthetic medium. *Solid State Ionics* 288, 240–243. doi:10.1016/j.ssi.2015.11.032

Phuc, N. H. H., Yamamoto, T., Muto, H., and Matsuda, A. (2017a). Fast synthesis of Li2S–P2S5–LiI solid electrolyte precursors. *Inorg. Chem. Front.* 4, 1660–1664. doi:10.1039/c7qi00353f

Preishuber-Pflugl, F., and Wilkening, M. (2016). Mechanochemically synthesized fluorides: local structures and ion transport. *Dalton Trans.* 45, 8675–8687. doi:10.1039/c6dt00944a

Schmaltz, T., Hartmann, F., Wicke, T., Weymann, L., Neef, C., and Janek, J. (2023). A roadmap for solid-state batteries. *Adv. Energy Mater.* 13. doi:10.1002/aenm.202301886

Stöffler, H., Zinkevich, T., Yavuz, M., Hansen, A.-L., Knapp, M., Bednarčík, J., et al. (2019). Amorphous versus crystalline Li3PS4: local structural changes during synthesis and Li ion mobility. *J. Phys. Chem. C* 123, 10280–10290. doi:10.1021/acs.jpcc.9b01425

Takahashi, M., Yang, S., Yamamoto, K., Ohara, K., Phuc, N. H. H., Watanabe, T., et al. (2021). Improvement of lithium ionic conductivity of Li3PS4 through suppression of crystallization using low-boiling-point solvent in liquid-phase synthesis. *Solid State Ionics* 361, 115568. doi:10.1016/j.ssi.2021.115568

Wan, T. H., Saccoccio, M., Chen, C., and Ciucci, F. (2015). Influence of the discretization methods on the distribution of relaxation times deconvolution: implementing radial basis functions with DRTtools. *Electrochimica Acta* 184, 483–499. doi:10.1016/j.electacta.2015.09.097

Yamamoto, K., Takahashi, M., Ohara, K., Phuc, N. H. H., Yang, S., Watanabe, T., et al. (2020). Synthesis of sulfide solid electrolytes through the liquid phase: optimization of the preparation conditions. *ACS Omega* 5, 26287–26294. doi:10.1021/acsomega.0c04307

Yamamoto, K., Yang, S., Takahashi, M., Ohara, K., Uchiyama, T., Watanabe, T., et al. (2021). High ionic conductivity of liquid-phase-synthesized Li3PS4 solid electrolyte, comparable to that obtained via ball milling. *ACS Appl. Energy Mater.* 4, 2275–2281. doi:10.1021/acsaem.0c02771